Kinematics Analysis and Implementation of a Motion-Following Task for a Humanoid Slave Robot Controlled by an Exoskeleton Master Robot

Deok Hui Song, Woon Kyu Lee, and Seul Jung*

Abstract: This article presents the kinematic analysis and implementation of an interface and control of two robots-an exoskeleton master robot and a human-like slave robot with two arms. Two robots are designed and built to be used for motion-following tasks. The operator wears the exoskeleton master robot to generate motions, and the slave robot is required to follow after the motion of the master robot. To synchronize the motions of two robots, kinematic analysis is performed to correct the kinematic mismatch between two robots. Hardware implementation of interface and control is done to test motion-following tasks. Experiments are performed to confirm the feasibility of the motion-following tasks by two robots.

Keywords: Kinematics, motion following, teleoperation control.

1. INTRODUCTION

Recently, occasions of interactive reaction between robots and humans have enormously increased in different types of environments as the technology of service robots is developed further [1-4]. There are several types of interaction between robots and human operators. Robot pets are a good interactive example between robots and humans through the exchange of their emotions. One simple interaction with robots is when they are used in tele-operated control tasks [5-7]. Using a joystick, an operator can control the movement of the slave robot with a visual feedback of the master robot movement. A human operator can control remotely located robots. Here, one basic requirement for the slave robot is the accurate motion following after the master moves.

For a motion-following task, the slave robot is required to follow after the movement of the master robot exactly. The operator wears the exoskeleton robot to generate motions. Then, as shown in Fig. 1, the slave robot is required to follow the motion after it is performed by the master robot.

To synchronize motions of two robots, several issues have to be solved. First, a kinematic analysis of the master and the slave has to be done to match both movements. Two robots are designed in slightly different configurations due to the actuator housing problems of the slave robot. The exoskeleton robot is not actuated by motors, thus it has a more flexible structure in design. The slave robot is actually actuated by motors commanded from the exoskeleton master robot by wireless communication. The different kinematic configuration leads to asynchronous movements in the Cartesian coordinates. To synchronize movements, kinematic analysis is required to compensate for mismatched parameters. Second, an interface between two robots has been implemented on a field programmable gate array (FPGA). Motion data from the master robot are collected and transferred to the slave robot. Finally, an accurate position control has to be done in the slave robot in order for it to follow the commanded trajectory.

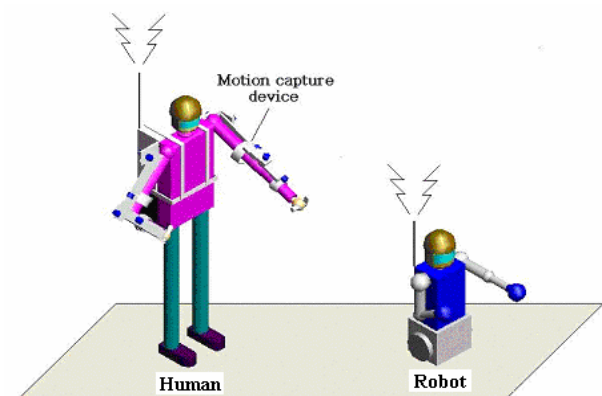In the framework of implementing motion-following tasks, two robots are built and their forward

Doek Hui Song, Woon Kyu Lee, and Seul Jung are with the BK 21 Mechatronics Group, Chungnam National University, 220 Gung-dong, Yuseon-gu, Daejeon 305-764, Korea (e-mails: hui314@yahoo.co.kr, seeuspace@hotmail.com, jungs@cnu.ac.kr).
* Corresponding author.

Fig. 1. Concept of motion-following task.

kinematics and inverse kinematics are analyzed. Kinematics differences between the two robots are compared and compensated in order to have synchronized motions. The movement of the exoskeleton master robot is captured by encoders mounted on each joint. Those encoder data are converted to joint angle values and those values are transferred to the slave robot to calculate end-effector positions. Those end-effector positions are used to calculate inverse kinematic solutions of the slave robot to generate desired joint values and command the slave robot to move. Next, the controller of the slave robot actuates and moves the arms. Encoder values of the slave robot are also used for calculating the position of the end-effector through forward kinematics.

In the simulation studies, two end-effector position values are compared to confirm that kinematic analysis is correct. Experimental studies of motion-following tasks are also conducted to confirm the performance of the motion-following task.

2. KINEMATICS ANALYSIS

2.1. Master and slave robots

Fig. 2 shows the exoskeleton master robot and the humanoid two-armed slave robot. The master robot has a total of 12 degrees–of-freedom(DOF). The master robot is designed in such a way that a human operator can wear it and move its arms. Movements of the master robot are captured by joint encoders. The slave robot also has 12 DOF. Each joint of the slave robot is actuated.
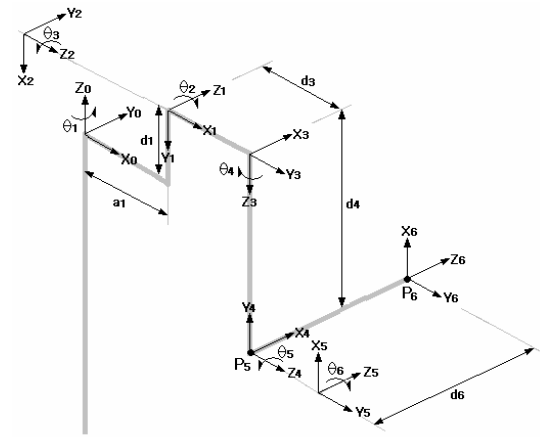
2.2. Forward kinematics

Fig. 3 shows the coordinate transforms of the master robot and slave robot, respectively [8]. Table 1 lists the D-H parameters for the master robot.
From the D-H parameters in Table 1, transformation matrices are obtained.
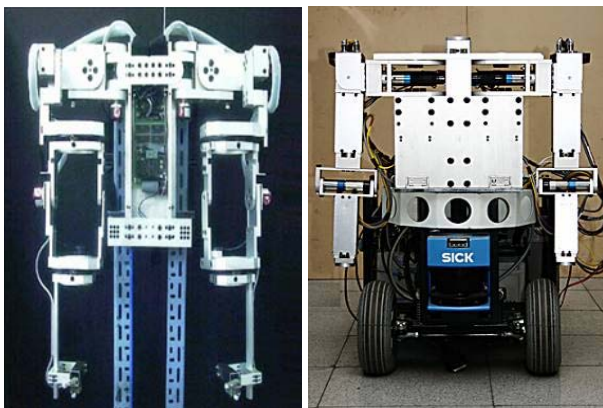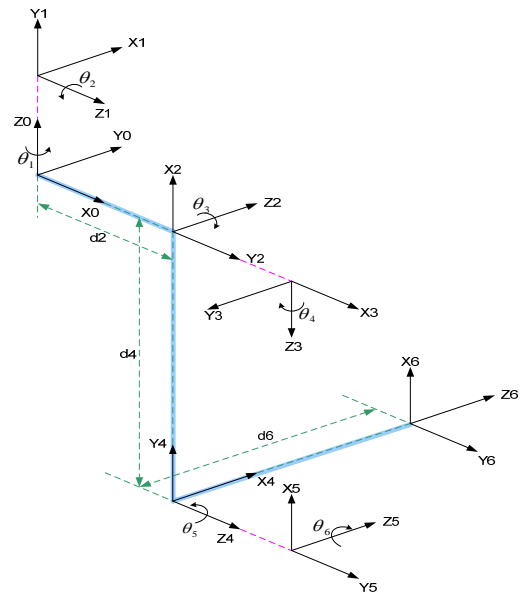

(a) Master robot.   (b) Slave robot.

Fig. 2. Master and slave robots.

(a) Master robot.

(b) Slave robot.

Fig. 3. Coordinates of two robots.

Table 1. D-H parameters and Joint range of the master robot.

Joint	θ_i	α_i	a_i	d_i	Joint range (degree)
1	0	-90	a_1	d_1	-45 to 45
2	90	90	0	0	-90 to 90
3	90	90	0	d_3	80 to 270
4	0	-90	0	d_4	-90 to 90
5	90	90	0	0	0 to 160
6	0	0	0	d_6	-90 to 90

$$
{}^0A_1 = \begin{bmatrix} C_1 & 0 & -S_1 & a_1C_1 \\ S_1 & 0 & C_1 & a_1S_1 \\ 0 & -1 & 0 & d_1 \\ 0 & 0 & 0 & 1 \end{bmatrix}, \quad {}^1A_2 = \begin{bmatrix} C_2 & 0 & S_2 & 0 \\ S_2 & 0 & -C_2 & 0 \\ 0 & 1 & 0 & 0 \\ 0 & 0 & 0 & 1 \end{bmatrix},
$$

$$^2A_3 = \begin{bmatrix} C_3 & 0 & S_3 & 0 \\ S_3 & 0 & -C_3 & 0 \\ 0 & 1 & 0 & d_3 \\ 0 & 0 & 0 & 1 \end{bmatrix}, \quad ^3A_4 = \begin{bmatrix} C_4 & 0 & -S_4 & 0 \\ S_4 & 0 & C_4 & 0 \\ 0 & -1 & 0 & d_4 \\ 0 & 0 & 0 & 1 \end{bmatrix},$$

$$^4A_5 = \begin{bmatrix} C_5 & 0 & S_5 & 0 \\ S_5 & 0 & -C_5 & 0 \\ 0 & 1 & 0 & 0 \\ 0 & 0 & 0 & 1 \end{bmatrix}, \quad ^5A_6 = \begin{bmatrix} C_6 & -S_6 & 0 & 0 \\ S_6 & C_6 & 0 & 0 \\ 0 & 0 & 1 & d_6 \\ 0 & 0 & 0 & 1 \end{bmatrix}, \tag{1}$$

where $c_i = \cos\theta_i, s_i = \sin\theta_i$.

Table 2 shows the D-H parameters of the slave robot.

We see from the two tables that the configurations of Joints 1 to 4 are different while the rest of the joint configuration is the same. This different configuration causes different movements of the end-effector position in the Cartesian space. The goal is to align the movement of two robots. The corresponding transformation matrices of the slave robot are shown in (2).

$$^0A_1 = \begin{bmatrix} C_1 & 0 & S_1 & 0 \\ S_1 & 0 & -C_1 & 0 \\ 0 & 1 & 0 & 0 \\ 0 & 0 & 0 & 1 \end{bmatrix}, \quad ^1A_2 = \begin{bmatrix} C_2 & 0 & S_2 & 0 \\ S_2 & 0 & -C_2 & 0 \\ 0 & 1 & 0 & d2 \\ 0 & 0 & 0 & 1 \end{bmatrix},$$

$$^2A_3 = \begin{bmatrix} C_3 & 0 & -S_3 & 0 \\ S_3 & 0 & C_3 & 0 \\ 0 & -1 & 0 & 0 \\ 0 & 0 & 0 & 1 \end{bmatrix}, \quad ^3A_4 = \begin{bmatrix} C_4 & 0 & -S_4 & 0 \\ S_4 & 0 & C_4 & 0 \\ 0 & -1 & 0 & d4 \\ 0 & 0 & 0 & 1 \end{bmatrix},$$

$$^4A_5 = \begin{bmatrix} C_5 & 0 & S_5 & 0 \\ S_5 & 0 & -C_5 & 0 \\ 0 & 1 & 0 & 0 \\ 0 & 0 & 0 & 1 \end{bmatrix}, \quad ^5A_6 = \begin{bmatrix} C_6 & -S_6 & 0 & 0 \\ S_6 & C_6 & 0 & 0 \\ 0 & 0 & 1 & d6 \\ 0 & 0 & 0 & 1 \end{bmatrix}. \tag{2}$$

The end-effector position can be obtained from the following matrix.

Table 2. D-H parameters and Joint range of the slave robot.

Joint	θ_i	α_i	a_i	d_i	Joint range (degree)
1	90	90	0	0	45 to 45
2	90	90	0	d_2	80 to 270
3	90	-90	0	0	0 to 90
4	-90	-90	0	d_4	-180 to 0
5	90	90	0	0	0 to 160
6	0	0	0	d_6	-90 to 90

$$^0T_6 = {^0A_6} = \begin{bmatrix} n_x & s_x & a_x & p_x \\ n_y & s_y & a_y & p_y \\ n_z & s_z & a_z & p_z \\ 0 & 0 & 0 & 1 \end{bmatrix} \tag{3}$$

2.3. Inverse kinematics
2.3.1 Inverse kinematics of the master robot

From Fig. 3(a), P_5 is given as

$$p_5 = p_6 - d_6 a$$
$$= \begin{bmatrix} (d_4C_2S_3 + d_3S_2 + a_1)C_1 + (d_4C_3)S_1 \\ (d_4C_2S_3 + d_3S_2 + a_1)S_1 + (-d_4C_3)C_1 \\ -d_4S_2S_3 + d_3C_2 + d_1 \end{bmatrix}, \tag{4}$$

where $a = [a_x\ a_y\ a_z]^T$.

Solutions of $\theta_1, \theta_2, \theta_3$ are analyzed as two cases when $\theta_2 = 0$ and $\theta_2 \neq 0$, depending upon the value of $\sin\theta_2$. The corresponding results are as follows:

i) $[\theta_2 = 0]$

$$\theta_1 = \tan^{-1}\left[\frac{Bp_{5x} \pm A\sqrt{A^2 + B^2 - p_{5x}^2}}{-Ap_{5x} \pm B\sqrt{A^2 + B^2 - p_{5x}^2}}\right], \tag{5}$$

$$\theta_2 = 0, \tag{6}$$

$$\theta_3 = \sin^{-1}\left[\frac{-E}{2D}\right]. \tag{7}$$

ii) $[\theta_2 \neq 0]$

$$\theta_1 = \tan^{-1}\left[\frac{Bp_{5x} \pm A\sqrt{A^2 + B^2 - p_{5x}^2}}{-Ap_{5x} \pm B\sqrt{A^2 + B^2 - p_{5x}^2}}\right], \tag{8}$$

$$\theta_2 = \tan^{-1}\left[\frac{FH \pm G\sqrt{G^2 + H^2 - F^2}}{-FG \pm H\sqrt{G^2 + H^2 - F^2}}\right], \tag{9}$$

$$\theta_3 = \tan^{-1}\left[\pm\frac{d_3C_2 + d_1 - p_{5z}}{\sqrt{1 - (d_3C_2 + d_1 - p_{5z})^2}}\right], \tag{10}$$

where

$$A \equiv d_4C_2S_3 + d_3S_2 + a_1,$$
$$B \equiv d_4C_3,$$
$$D \equiv d_4C_2a_1,$$
$$E \equiv a_1^2 + d_4^2 - p_{5x}^2 - p_{5y}^2,$$
$$F \equiv 2d_3a_1,$$
$$G \equiv 2a_1(d_1 - p_{5z}),$$
$$H \equiv p_{5x}^2 + p_{5y}^2 - d_4^2 - d_3^2 + (d_1 - p_{5z})^2 - a_1^2.$$

Solutions for $\theta_4, \theta_5, \theta_6$ are given as

$$\theta_4 = \tan^{-1}\left[\frac{I}{J}\right], \tag{11}$$

$$\theta_5 = \tan^{-1}\left[\frac{K}{L}\right], \tag{12}$$

$$\theta_6 = \tan^{-1}\left[\frac{M}{N}\right], \tag{13}$$

where

$$I \equiv C_1 S_2 a_x + S_1 S_2 a_y + C_2 a_z,$$

$$J \equiv (C_1 C_2 C_3 - S_1 S_3) a_x + (S_1 C_2 C_3 + C_1 S_3) a_y$$
$$\quad - S_2 C_3 a_z,$$

$$K \equiv [(C_1 C_2 C_3 - S_1 S_3) C_4 + C_1 S_2 S_4] a_x$$
$$\quad + [(S_1 C_2 C_3 + C_1 S_3) C_4 + S_1 S_2 S_4] a_y$$
$$\quad + (-S_2 C_3 C_4 + C_2 S_4) a_z,$$

$$L \equiv (C_1 C_2 S_3 + S_1 C_3) a_x + (S_1 C_2 S_3 - C_1 C_3) a_y$$
$$\quad - S_2 S_3 a_z,$$

$$M \equiv [-(C_1 C_2 C_3 - S_1 S_3) S_4 + C_1 S_2 C_4] n_x$$
$$\quad + [-(S_1 C_2 C_3 + C_1 S_3) S_4 + S_1 S_2 C_4] n_y$$
$$\quad + (S_2 C_3 S_4 + C_2 C_4) n_z,$$

$$N \equiv [-(C_1 C_2 C_3 - S_1 S_3) S_4 + C_1 S_2 C_4] s_x$$
$$\quad + [-(S_1 C_2 C_3 + C_1 S_3) S_4 + S_1 S_2 C_4] s_y$$
$$\quad + (S_2 C_3 S_4 + C_2 C_4) s_z,$$

2.3.2 Inverse kinematics of the slave robot

i) $\theta_1, \theta_2, \theta_3$

$$p = p_6 - d_6 a = (p_x, p_y, p_z)^T$$
$$= \begin{bmatrix} d_4(S_1 C_3 - C_1 C_2 S_3) + d_2 S_1 \\ -d_4(C_1 C_3 + S_1 C_2 S_3) - d_2 C_1 \\ -d_4 S_2 S_3 \end{bmatrix}, \tag{14}$$

where $a = [a_x, a_y, a_z]^T$.
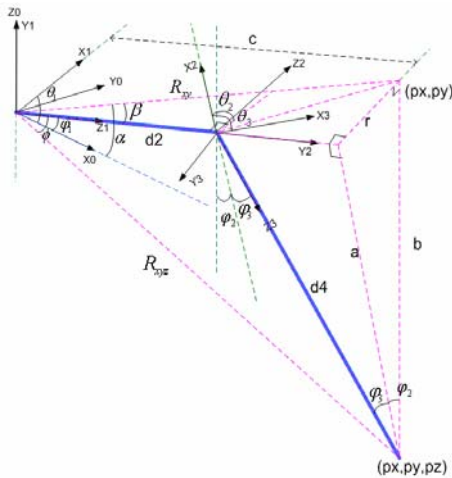
Fig. 4. Solutions for joints 1, 2, and 3 of the slave.

From Fig. 4, we have

$$\varphi_1 = \tan^{-1}\frac{p_y x \mp p_x r}{p_x x \pm p_y r}, \tag{15}$$

$$\varphi_2 = \tan^{-1}\frac{r}{|b|}, \tag{16}$$

$$\varphi_3 = \tan^{-1}\frac{c - d_2}{a}, \tag{17}$$

where

$$R_{xyz} = \sqrt{p_x^2 + p_y^2 + p_z^2}, \quad c = \frac{R_{xyz}^2 + d_2^2 - d_4^2}{2d_2},$$

$$r = \sqrt{p_x^2 + p_y^2 - c^2}, \quad b = p_z, \quad a = \sqrt{R_{xyz}^2 - c^2}.$$

Therefore, $\theta_1, \theta_2, \theta_3$ are calculated as

$$\theta_1 = \pi/2 \pm \varphi_1, \tag{18}$$
$$\theta_2 = \pi/2 \pm \varphi_2, \tag{19}$$
$$\theta_3 = \pi/2 - \varphi_3. \tag{20}$$

ii) $\theta_4, \theta_5, \theta_6$

The remaining three joints $\theta_4, \theta_5, \theta_6$ are also obtained as

$$\theta_4 = \tan^{-1}\left(\frac{\sin\theta_4}{\cos\theta_4}\right), \tag{21}$$

$$\theta_5 = \frac{\pi}{2} + \tan^{-1}\left(\frac{\sin\theta_5}{\cos\theta_5}\right), \tag{22}$$

$$\theta_6 = \tan^{-1}\left(\frac{\sin\theta_6}{\cos\theta_6}\right), \tag{23}$$

where

$$\sin\theta_4 = -C_1 S_2 a_x - S_1 S_2 a_y + C_2 a_z,$$

$$\cos\theta_4 = (C_1 C_2 C_3 + S_1 S_3) a_x + (S_1 C_2 C_3 - C_1 S_3) a_y$$
$$\quad + S_2 C_3 a_z,$$

$$\sin\theta_5 = (C_1 C_2 S_3 - S_1 C_3) a_x + (S_1 C_2 S_3 + C_1 C_3) a_y$$
$$\quad + S_2 S_3 a_z,$$

$$\cos\theta_5 = (C_1 C_2 C_3 C_4 + S_1 S_3 C_4 - C_1 S_2 S_4) a_x$$
$$\quad + (S_1 C_2 C_3 C_4 - C_1 S_3 C_4 - S_1 S_2 S_4) a_y$$
$$\quad + (S_2 C_3 C_4 - S_2 S_3) a_z,$$

$$\sin\theta_6 = -(C_1 C_2 C_3 S_4 + S_1 S_3 S_4 + C_1 S_2 C_4) n_x$$
$$\quad - (S_1 C_2 C_3 S_4 - C_1 S_3 S_4 + S_1 S_2 C_4) n_y$$
$$\quad - (S_2 C_3 S_4 - C_2 C_4) n_z,$$

$$\cos\theta_6 = -(C_1 C_2 C_3 S_4 + S_1 S_3 S_4 + C_1 S_2 C_4) s_x$$
$$\quad - (S_1 C_2 C_3 S_4 - C_1 S_3 S_4 + S_1 S_2 C_4) s_y$$
$$\quad - (S_2 C_3 S_4 - C_2 C_4) s_z.$$

3. SIMULATION OF KINEMATICS

3.1. Slave robot

To confirm the kinematics analysis presented in the previous section, simulations of the slave robot are conducted. Here, for given joints' angle values, the end-effector position is obtained by the forward kinematics. Next, inverse kinematics solves the solutions for joint angles again. These joints angles are used to calculate the end-effector position and are compared with given joint angle values. Fig. 5 shows several movements of each joint. We see that end-effector positions are exactly matched for two calculations using forward and inverse kinematics.

Fig. 6 shows the movement of all joints. We see that the end-effector position is exactly matched.

(a) Joint 1.

(b) Joint 2.

(c) Joint 3.

(d) Joint 4.

(e) Joint 5.

(f) Joint 6.
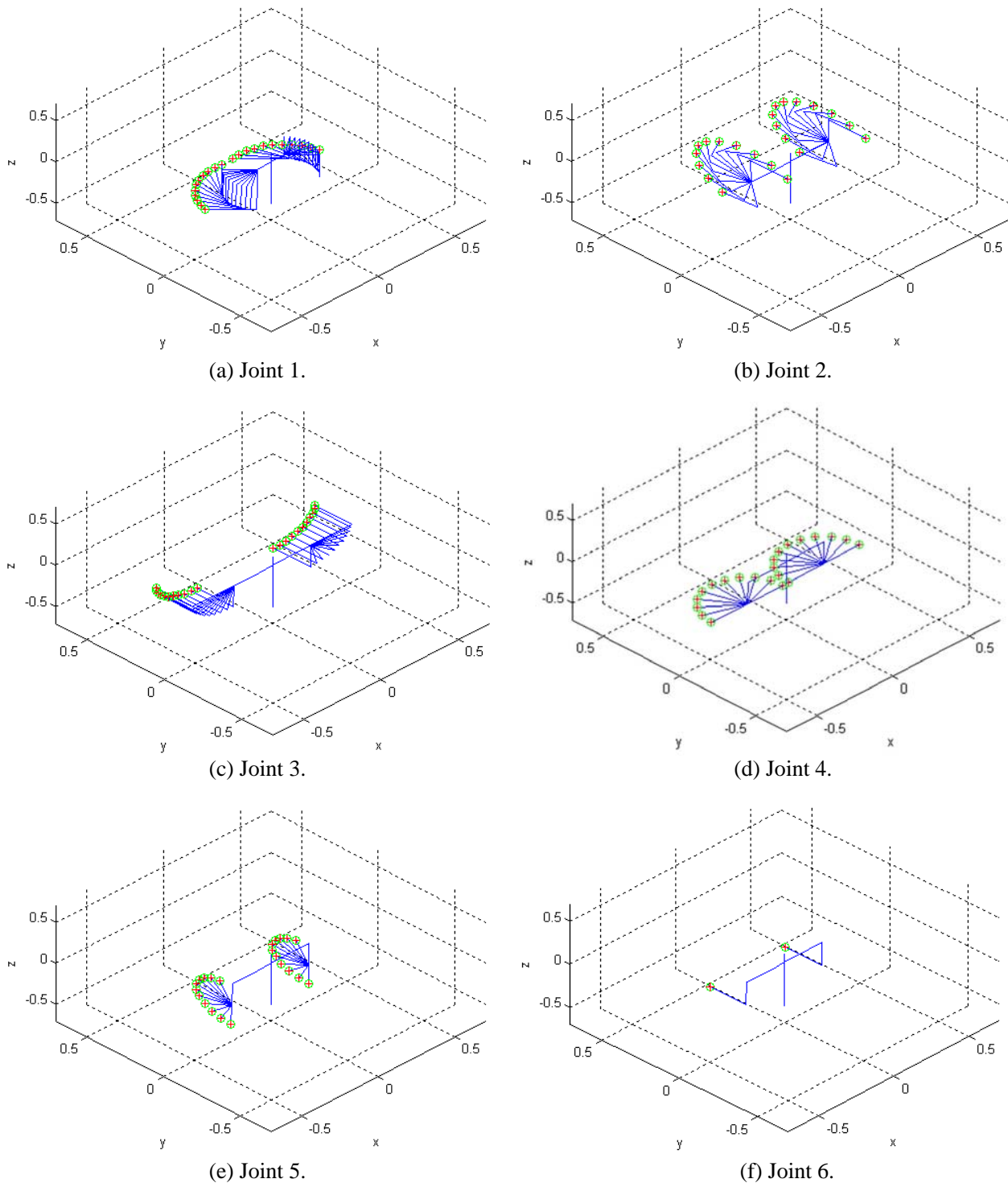
Fig. 5. Simulation results of inverse kinematics.
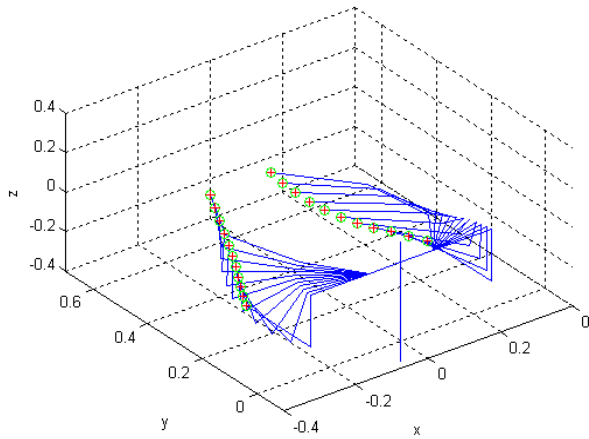
Fig. 6. Movements of all joints.

This simulation confirms that the kinematic analysis of the slave robot is correct. Simulation and confirmation for the master robot have been already presented in our previous research [8].

4. MAPPING BETWEEN TWO ROBOTS

4.1. Kinematic mapping

Table 3 shows the D-H parameters of two robots. We clearly see that joint 1 through joint 3 are different from the two robots. Different rotating frame yields different D-H parameters as well as different arm lengths.

Because the workspace of the slave robot is slightly smaller than that of the master robot, we should find the factor that scales the movement in the Cartesian space. We have followed the next procedure:
1. First, the two base coordinates are aligned together by moving the z axis of the master robot by the length of d_1
2. Second, the ratio of the link length is found. We have found scaling values at 0.64, 0.6875, and 0.625 for each axis of the first three links.

These values are obtained by comparing each link length. These factors are multiplied to the Cartesian position of the exoskeleton robot after obtaining the transformation matrix $T = {}^0A_6$.

Table 3. Comparison of the D-H parameters of two robots.

Link	Exoskeleton (m)		Robot manipulator (m)	
	a_i	d_i	a_i	d_i
1	0.1	0.05	0	0
2	0	0	0	0.16
3	0	0.15	0	0
4	0	0.4	0	0.275
5	0	0	0	0
6	0	0.4	0	0.25

4.2. Mapping experiments

In this paper, we move the master robot with arbitrary trajectories. First, encoder data from the master robot are obtained. These data are used to calculate the end-effector position of the master robot. Afterwards, scale it down by the factor. These scaled down values are used to calculate joint values of the slave robot by inverse kinematics. Then, the end-effector position of the slave robot is calculated and plotted. Fig. 7 shows the movement of two robots in
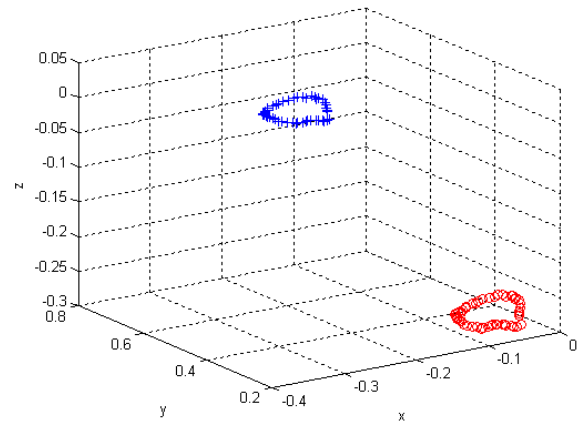
(a) End-effector positions.
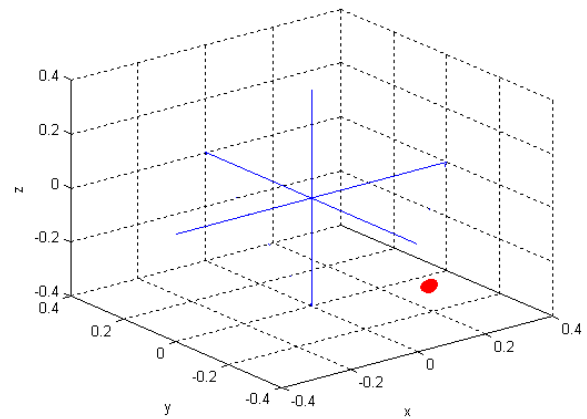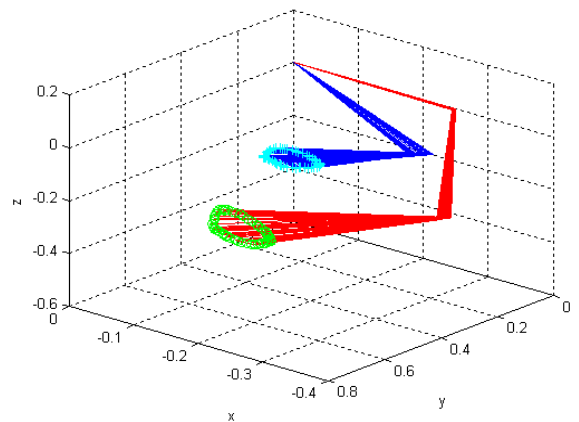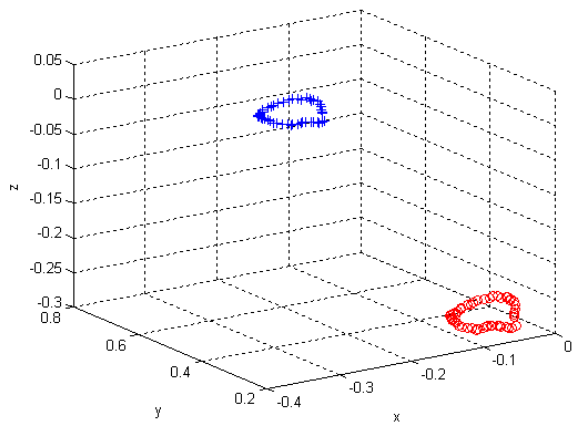

(b) Positional mismatching errors.

(c) Real end-effector position of two robots.

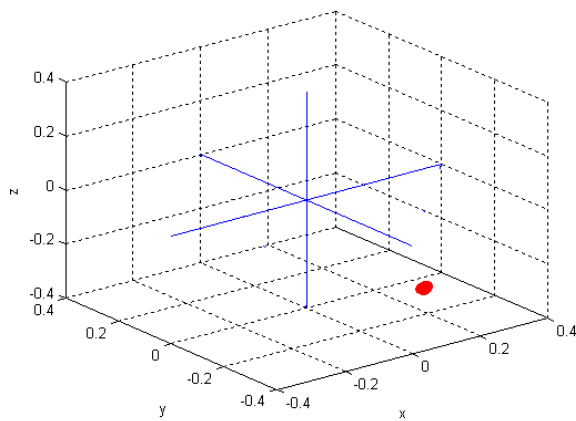Fig. 7. Experiment 1: Without correction of mapping.

the Cartesian space.

4.2.1 Without correction of mapping

The first experiment is tested and two robot movements are plotted without any mapping correction. We clearly see from Fig. 7(a) that movements of the two robots are separately plotted in the Cartesian space due to the different kinematics. Mapping errors are indicated far away from the origin as shown in Fig. 7(b). The plot of Fig. 7(c) shows the
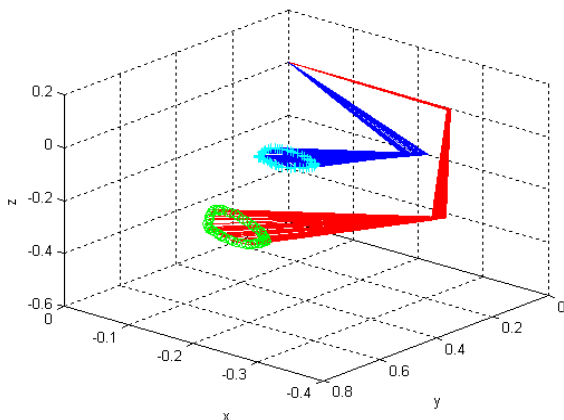
end-effector position of two robots.

4.2.2 With correction of mapping

Next, an experiment is conducted for the master robot by moving the arbitrary trajectories. The movements of two robots are plotted in Fig. 8(a). We see that movements of the two robots are exactly matched, such that mapping errors are zero as shown in Fig. 8(b).

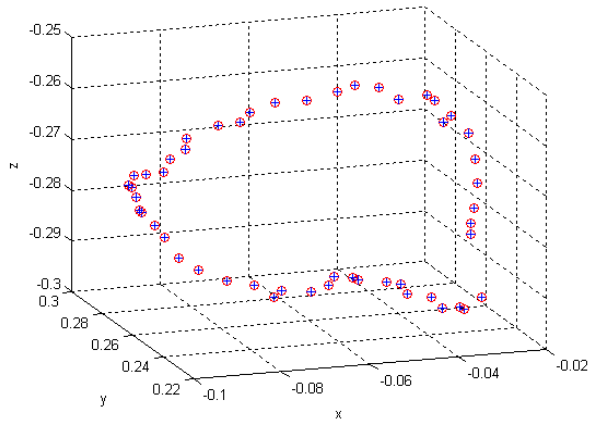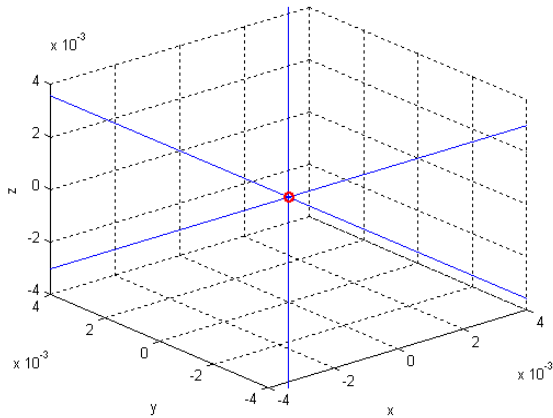To see the map matching performance for other
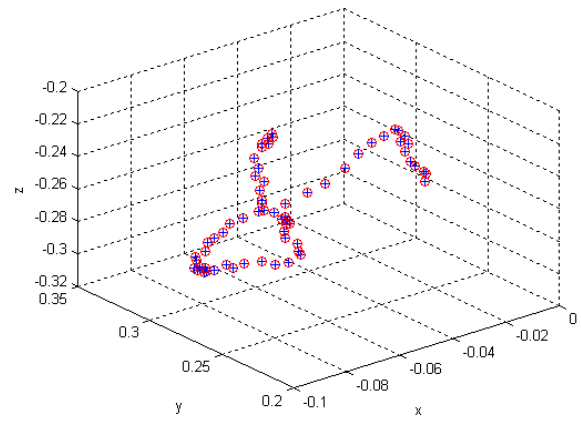
(a) End-effector positions.
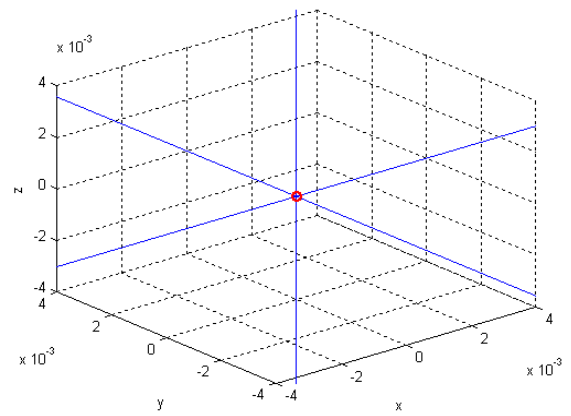
(a) End-effector positions.

(b) Positional mismatching errors.

(b) Positional mismatching errors.

(c) Real end-effector position of two robots.

(c) Real end-effector position of two robots.
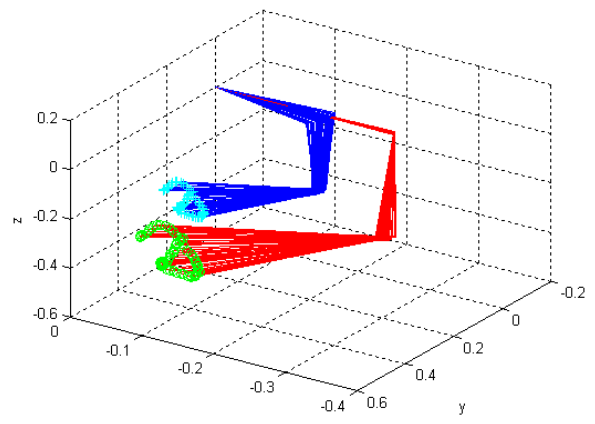
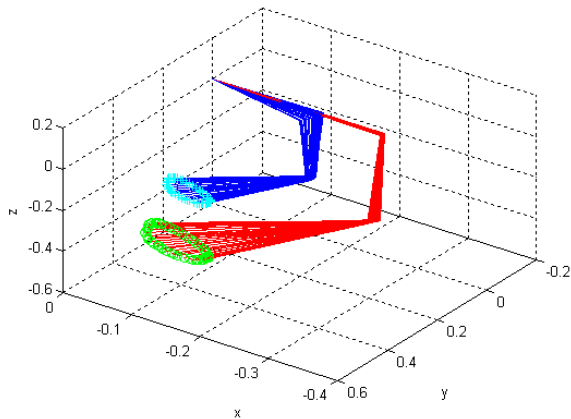Fig. 7. Experiment 1: Without correction of mapping.

Fig. 8. Experiment 2: With correction of mapping.

(a) End-effector positions.

(b) Positional mismatching errors.

(c) Real end-effector position of two robots.

Fig. 9. Experiment 3: With correction of mapping.

movements, another movement of two robots is tested as shown in Fig. 9. Positional errors are very small within 0.002m in Fig. 9(b). Two robot movements are plotted in Fig. 9(c).

5. MOTION-FOLLOWING EXPERIMENTS

In this section, the operator wears the master robot and generates arbitrary motions. The slave robot is required to follow after the operator. As the operator
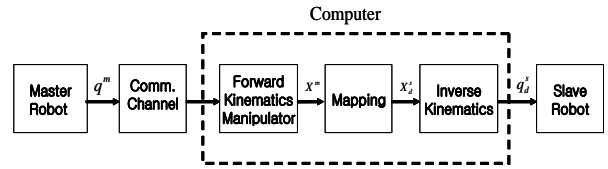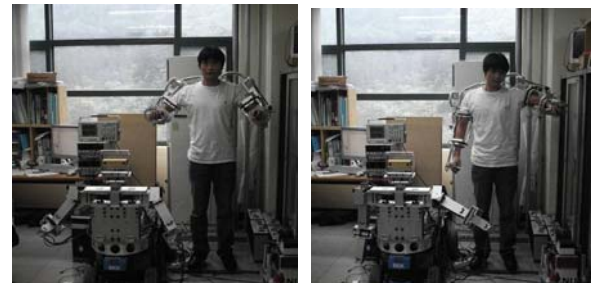

Fig. 10. Experiments of motion-following tasks.

(a) Initial position.   (b) Two arms are folded.

(c) Two arms are spread.   (d) Left arm is lifted.

Fig. 11. Experiments of motion-following tasks.

moves continuously, the slave robot also keeps following the movement. To actuate the slave robot, an interface and a control are implemented on FPGAs between two robots. Captured joint angle data are transferred to the slave robot to command the movement of the slave robot.

The block diagram of controlling the slave robot is shown in Fig. 10. The master robot joint movement data q^m are gathered by an FPGA chip and transferred to the slave side through the communication channel. Then, in the slave side, the Cartesian position X^m of the master robot is calculated and the mapped position X_d^s of the slave robot is calculated through the mapping process. Finally, inverse kinematics solves the desired joint command values q_d^s from X_d^s.

The tracking error becomes $e^s = q_d^s - q^s$ and forms proportional-integral-derivative controller for each joint of the slave robot. Suitable PID controller gains are selected by trial and error experiments. Experiments of motion-following demonstration are shown in Fig. 11. Four figures are captured from the actual continuous movements of moving pictures.
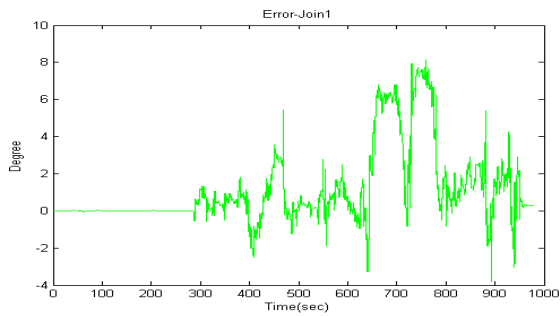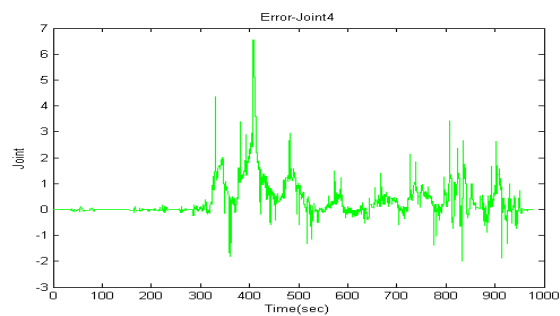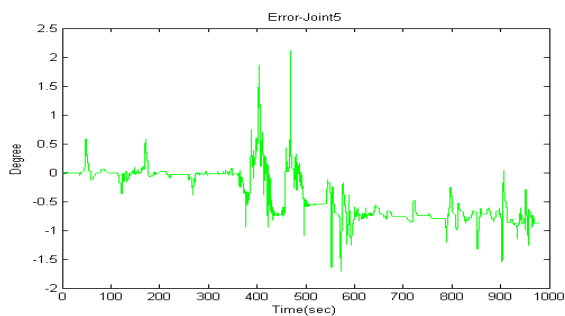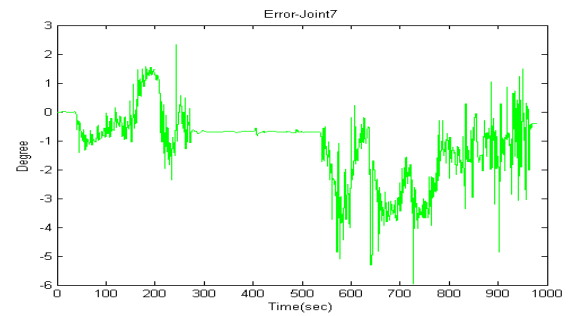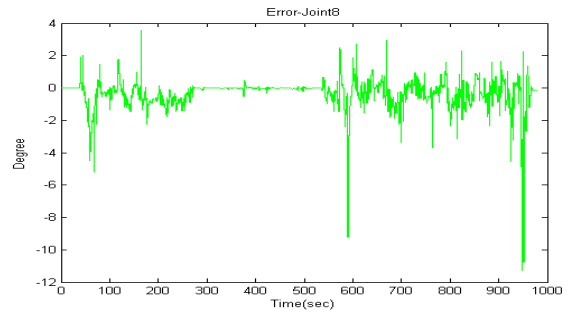
(a) Joint 1.
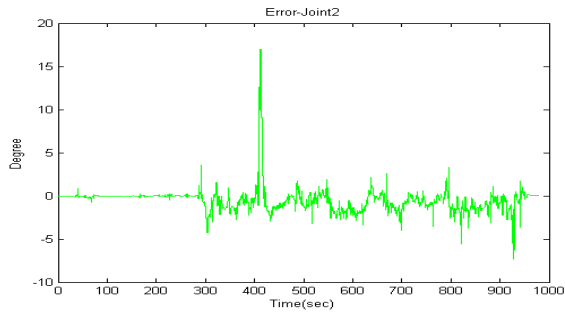
(b) Joint 2.
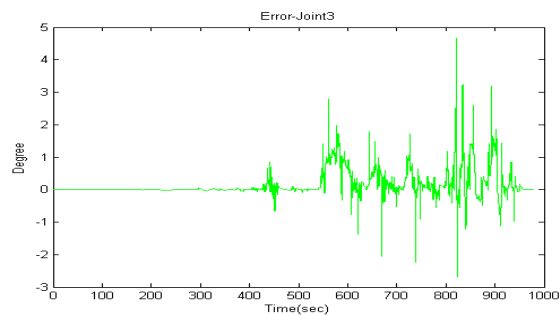
(c) Joint 3.

(d) Joint 4.

(e) Joint 5.

Fig. 12. Tracking errors of the left arm of two robots.

(a) Joint 1.

(b) Joint 2.

(c) Joint 3.

(d) Joint 4.
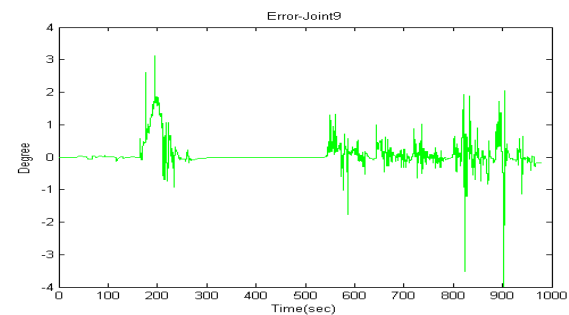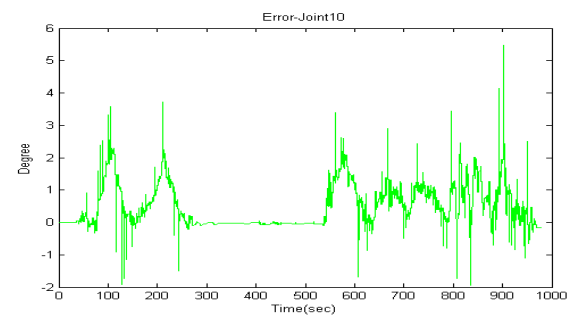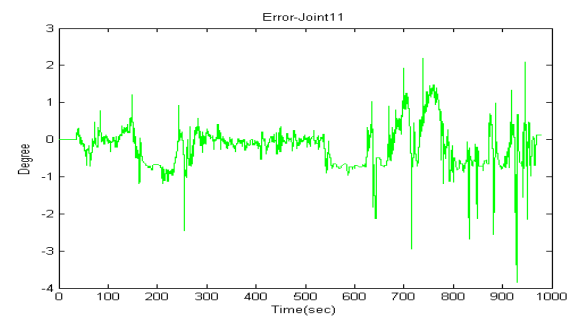
(e) Joint 5.

Fig. 13. Tracking errors of the right arm of two robots.

To clearly compare the results of motion-following movements between the master and the slave robot, joint tracking errors between the master joint q^m and the slave joint movement q^s of all joints are plotted in Figs. 12 and 13, which show the tracking errors of the left arm and the right arm, respectively.

We see that the mean tracking errors are close to zero. A larger error occurs in joint 1 since joint 1 carries all the loads from other joints. Because joint 6 is the rotation of the end-effector whose error is very small, the plot is omitted.

6. CONCLUSION

This article presented the hardware implementation of interface and control between two robots for motion-following tasks in the framework of tele-operation tasks. To synchronize motions, a kinematics mapping between two robots was analyzed and compensated. Simulation and experimental results confirmed that the mapping analysis is quite effective. However, we noticed that the slave robot has a limited bandwidth due to the time consuming calculation of inverse kinematics and its own mechanical bandwidth. Accurately controlling the slave robot with PID controllers is one important issue that needs to be solved in the near future since the slave robot arms are nonlinear.

REFERENCES

[1] S. H. Chang, J. T. Kim, J. H. Borm, C. W. Lee, and J. O. Park, "KIST teleoperation system for humanoid robot," *Proc. of IEEE/RSJ Conf. on Intelligent Robots and Systems*, vol. 2, pp. 1198-1203, 1999.

[2] M. Oda, T. Doi, and K. Wakata, "Tele-manipulation of a satellite mounted robot by an on-ground astronaut," *Proc. of IEEE Conf. on Robotics and Automations*, pp. 1891-1896, 2001.

[3] J. Funda, R. H. Taylor, S. Gomory, and K. G. Gruben, "Constrained catesian motion control for teleoperated surgical robots," *IEEE Trans. on Robotics and Automations*, vol. 12, no. 3, pp. 453-465, 1996.

[4] T. Mori, K. Tsujioka, and T. Sato, "Human-like action recognition system on whole body motion-captured file," *Proc. of IEEE Conf. on International Conference on Intelligent Robots and Systems*, Hawaii, USA, pp. 2066-2073, 2001.

[5] S. Jung, P. W. Jeon, and H. T. Cho, "Interface between robot and human: Application to boxing robot," *Proc. of the 2nd IFAC Conference on Mechatronic Systems*, 2002.

[6] P. W. Jeon, P. S. Jang, B. K. Ju, K. H. Cho, and S. Jung, "Development of boxing robot system for mechatronics education," *Proc. of Korean Automatic Control Conference* (in Korean), 2000.

[7] K. S. Fu, R. C. Gonzalez, and C. S. G. Lee, *ROBOTICS: Control, Sensing, Vision, and Intelligence*, McGraw-Hill, 1987.

[8] P. W. Jeon and S. Jung, "Teleoperated control of mobile robot using exoskeleton type motion capturing device through wireless communica-tion," *Proc. of IEEE/ASME Advanced Intelligent Mechatronics*, vol. 2, pp. 1107-1112, 2003.

Deok Hui Song received the B.S. and M.S. degrees in Mechatronics Engineering from Chungnam National University in 2002 and 2005, respectively. He is now working at the Korea Atomic Energy Research Institute in Daejeon, Korea. His interests include intelligent control and robotics.

Woonkyu Lee received the B.S. and M.S. degrees in Mechatronics Engineering from Chungnam National University in 2003 and 2005, respectively. He is now working at the Dodam Company in Daejeon, Korea. His research interests includes man-machine interface, SOC design, and mobile robotics.

Seul Jung received the B.S. degree in Electrical and Computer Engineering from Wayne State University in 1988, and the M.S. and Ph.D. degrees in Electrical and Computer Engineering from the University of California, Davis in 1991 and 1996, respectively. In 1997, after working at the Advanced Highway Maintenance and Construc-tion Technology Center, he joined the Department of Mechatronics Engineering in Chungnam National University where he is now an Associate Professor. He has been engaged in research and teaching in the area of intelligent robot systems, control and signal processing systems, and embedded digital systems. He has published over 90 international papers on these subjects. His research interests include intelligent systems, hardware imple-mentation of intelligent controllers, and human-oriented robotic systems. He is a Member of *Tau Beta Pi* and *Eta Kappa Nu*.